Dalton Transactions

Accepted Manuscript

ROYAL SOCIETY OF CHEMISTRY

www.rsc.org/dalton

Cyclometallated platinum(II) complexes containing NHC ligands; synthesis, characterization, photophysics and their application as emitters in OLEDs

A. I. Solomatina,[1] D. V. Krupenya,[1] V. V. Gurzhiy,[2] I. Zlatkin, [1] A. P. Pushkarev,[3] M. N. Bochkarev,[3] N. A. Besley,[4] E. Bichoutskaia,[4] S. P. Tunik[1]*

[1] Saint-Petersburg State University, Institute of Chemistry, Saint-Petersburg, Universiteskii pr. 26, 198504, Russian Federation, tel/fax: +7 (812) 3241258, e-mail: stunik@inbox.ru

[2] Saint-Petersburg State University, Institute of Earth Sciences, Saint-Petersburg, University emb. 7/9, 199034, Russian Federation, Tel: +7 (812) 3506688, e-mail: vladgeo17@mail.ru

[3] G. A. Razuvaev Institute of Organometallic Chemistry of Russian Academy of Sciences, Tropinina 49, 603950 Nizhny Novgorod, Russian Federation. Fax: +7 (831) 4627497; e-mail: mboch@iomc.ras.ru

[4] School of Chemistry, University of Nottingham, University Park, Nottingham NG7 2RD, UK tel. +44 (115) 8468465; e-mail: Elena.Bichoutskaia@nottingham.ac.uk

Abstract

A series of square planar [Pt(N^C)(NHC)L] complexes containing cyclometallated N^C ligands (phenylpyridine and benzoquinoline) and N-heterocyclic carbene (NHC): N^C = 2-phenylpyridine, 7,8-benzoquinoline; NHC= 1,3-dibenzylbenzimidazolium, 1,3-diethylbenzimidazolium, 1,3-dibenzylimidazolium; L = Cl, Br, -C_2Ph; has been synthesized in moderate to good yield. The complexes obtained were characterized using chemical analysis, MS-ESI spectrometry, NMR spectroscopy and X-ray crystallography. The complexes display moderate to strong phosphorescence in solution (Q. Y. 0.3-7.9 %) and in solid state (Q. Y. 2.7-16.0 %), which are related to metal modulated intraligand π–π* transitions located at aromatic system of cyclometallated ligands with some contribution of MLCT excited state. Emission lifetimes fall in the range 0.2-1.5 μs in solution and amount up to 13 μs in solid state. Analysis of the spectroscopic data together with the density functional theory (DFT) and time-dependent

density functional theory (TD DFT) calculations clearly support this assignment and show negligible contribution of the auxiliary ligands into emissive excited states. The compounds obtained were also used to prepare organic light emitting diode (OLED) devices, which display good luminance efficiency emitting in green area of the visible spectrum.

Introduction

Organometallic tetra-coordinated Pt(II) complexes have been extensively studied for more than one hundred years and now encompass a wide variety of compositional and structural archetypes incorporating a wide variety of organic ligands. However, in the last decades a few types of these complexes have attracted increased attention due to their extremely interesting and useful photophysical properties. Among these complexes, compounds based on cyclometallated N^C, N^C^N, N^N^C ligands[1–4] and those containing N-heterocyclic carbenes (NHC)[5–8] are of particular interest. The stability of these complexes in various media and under different conditions, high yield of triplet emission due to effective intersystem crossing stimulated by the heavy atom effect, easily tunable emission energy controlled by the variations in the electronic and steric characteristics of the ligand sphere make this type of Pt(II) compounds attractive for utilization in the phosphorescence organic light emitting diode (OLED) technology[1,2,9], biomedical[10–12] and sensoric[7,13] applications. It has been shown, both experimentally and theoretically, that the cyclometallated ligands play a key role in emission of these complexes[2,3]. The phosphorescence observed is due to a platinum atom modulated intraligand transitions, ^{3}IL ($\pi\rightarrow\pi^*$), excited state being centered at the cyclometallated ligand with some admixture of metal-to-ligand charge transfer, ^{3}MLCT ($d_\pi(Pt)\rightarrow\pi^*$). It was also demonstrated that the NHC ligands are not spectators in the emission processes and may modify the phosphorescence quantum yield (QY) considerably, depending on their electronic[8] and steric[6] properties. In the present paper we describe the synthesis, characterization and investigation of the photophysical and electroluminescence (EL) characteristics of a systematic range of neutral [Pt(N^C)(NHC)L] complexes, N^C = 2-phenylpyridine, 7,8-benzoquinoline; NHC= 1,3-dibenzylbenzimidazolium, 1,3-diethylbenzimidazolium, 1,3-dibenzylimidazolium; L = Cl, Br, -C_2Ph. The electronic structure of the compounds under study is characterized using density functional theory (DFT) calculations, with the time-dependent density functional theory (TDDFT) method used to assign the nature of orbitals responsible for the emission observed. The compounds obtained were used to prepare OLED devices, which displayed a fairly bright green luminescence at low voltage.

Experimental

Phenylacetylene, 2-phenylpyridine, 7,8-benzoquinoline were commercially available and used without additional purification. Solvents were purified and distilled using standard procedures. The platinum(II) precursor complexes [Pt(N^C)(DMSO)Cl] were prepared according to a published procedure,[14] and the imidazolium salts were synthesized according to the reported procedures.[15–17] The Ag(I) complexes with N-heterocyclic carbene were prepared in general method.[18] The solution ^{1}H, and 2D ^{1}H-^{1}H COSY NMR spectra were recorded by a Bruker DPX 300 and Bruker Avance 400 spectrometers. Mass spectra were measured on a Bruker micrOTOF 10223 instrument in the ESI^{+} mode (solvent – MeOH). Elemental analyses were carried out with Eurovector Euro-EA3028-HT.

Synthesis of [Pt (N^C-ppy)(1,3-dibenzylbenzimidazol-2-yliden)Br] (1)

[Pt(N^C-ppy)(DMSO)Cl] (70 mg, 0.151 mmol) and [Ag(1,3-dibenzylbenzimidazol-2-yliden)Br] (97 mg, 0.200 mmol) was added to 18 ml degassed CH_2Cl_2, and the reaction mixture was stirred at room temperature overnight. Gray precipitate was filtered off through Celite and the solvent removed using a rotary evaporator. The resulting product was added to 10 ml of KBr (500 mg, 4.20 mmol) solution in DMSO. The reaction mixture was heated at 100 $^{\circ}$C for 24h. After cooling to room temperature distilled water was added dropwise to the reaction mixture. The resulting yellow precipitate was filtered off, dried under vacuum and purified by column chromatography on Silica using CH_2Cl_2 as eluant. Yield: 71 mg (65%). Anal. Calcd for $C_{32}H_{26}BrN_3Pt$: C, 52.83; H, 3.60; N, 5.78. Found: C, 52.77; H, 3.72; N, 5.59%. ^{1}H NMR (300 MHz, $CDCl_3$, 298 K): δ 9.85 (d with broad ^{195}Pt satellites, $J_{H\text{-}H}$ = 5.6 Hz, 1H), 7.86 (t, $J_{H\text{-}H}$ = 7.7 Hz, 1H), 7.76 (d, $J_{H\text{-}H}$ = 7.9 Hz, 1H), 7.57 (d, $J_{H\text{-}H}$ = 8.0 Hz, 1H), 7.53 (d, $J_{H\text{-}H}$ = 6.9 Hz, 4H), 7.26-7.06 (m, 12H), 6.94 (t, $J_{H\text{-}H}$ = 7.4 Hz, 1H), 6.63 (dd, $J_{H\text{-}H}$ = 7.6, $J_{Pt\text{-}H}$ = 70 Hz, 1H), 6.08 (dd, $J_{H\text{-}H}$ = 59.3, 15.5 Hz, 4H). MS ESI (*m*/*z*): 647.18 $[M\text{-}Br]^{+}$, 749.09 $[M+Na]^{+}$, 766.06 $[M+K]^{+}$.

Synthesis of [Pt (N^C-ppy)(1,3-dibenzylbenzimidazol-2-yliden)Cl] (2)

The compound was prepared according to the procedure described for **1**, except that KCl (500 mg, 6.71 mmol) was used instead of potassium bromide. Yield: 69 mg (66%). Anal. Calcd for $C_{32}H_{26}ClN_3Pt$: C, 56.26; H, 3.84; N, 6.15.Found: C, 55.89; H, 4.09; N, 6.31%. ^{1}H NMR (300 MHz, $CDCl_3$, 298 K): δ 9.66 (d with broad ^{195}Pt satellites, $J_{H\text{-}H}$ = 5.1, 1 H), 7.87 (t, $J_{H\text{-}H}$ = 7.3 Hz, 1H), 7.76 (d, $J_{H\text{-}H}$ = 7.8 Hz, 1H), 7.67-7.45 (m, 5H), 7.33-7.05 (m, 12H), 6.94 (t, $J_{H\text{-}H}$ = 7.2 Hz, 1H), 6.69 (dd, $J_{H\text{-}H}$ = 7.4, $J_{Pt\text{-}H}$ = 70 Hz, 1H), 6.10 (dd, $J_{H\text{-}H}$ = 70.5, 15.5 Hz, 4H). MS ESI (*m*/*z*): 647.18 $[M\text{-}Cl]^{+}$, 706.14 $[M+Na]^{+}$, 722.10 $[M+K]^{+}$, 1330.32 $[2M\text{-}Cl]^{+}$.

Synthesis of [Pt (N^C-ppy)(1,3-dibenzylbenzimidazol-2-yliden)(C_2Ph)] (3)

35 mg (0,048 mmol) of **1**, 5 mg (0,048 mmol) phenylacetylene and 1mg CuI was added to the degassed mixture of CH_2Cl_2(20 ml)/diisopropylamine(7 ml). The reaction mixture was stirred overnight. The solvent was removed using a rotary evaporator. The product was dissolved in 40 ml dichloromethane and washed with water. The separated organic phase was dried over Na_2SO_4. Recrystallization from dichloromethane/hexane mixture gave the product as yellow crystals. Yield: 28 mg (78%). Anal. Calcd for $C_{40}H_{31}N_3Pt$: C, 64.16; H, 4.17; N, 5.61. Found: C, 64.62; H, 4.14; N, 5,31%. ^{1}H NMR (300 MHz, $CDCl_3$, 298 K): δ 9.89 (d, J_{H-H} = 5.2, 1H), 7.85 (t, J_{H-H} = 7.0 Hz, 1H), 7.78 (d, J_{H-H} = 7.8 Hz, 1H), 7.70-7.58 (m, 5H), 7.44 (d, J_{H-H} = 7.4 Hz, 2H), 7.27-7.07 (m, 15H), 7.04 (t, J_{H-H} = 7.3 Hz, 1H), 6.86 (dd, J_{H-H} = 7.2, J_{Pt-H}= 40 Hz, 1H), 6.08 (dd, J_{H-H} = 242.2, 15.5 Hz, 4H). MS ESI (*m*/*z*): 647.18 $[M-CCPh]^+$, 771.21 $[M+Na]^+$, 787.18 $[M+K]^+$.

Synthesis of [Pt (N^C-bzq)(1,3-dibenzylbenzimidazol-2-yliden)Br] (4)

The compound was prepared according to the procedure described for **1** using [Pt (N^C-bzq)dmsoCl] (74 mg, 0,151 mmol) as starting material. Yield: 66 mg (58%)**.** Anal. Calcd for $C_{34}H_{26}BrN_3Pt$: C, 54.33; H, 3.49; N, 5.59. Found: C, 54.28; H,3.44; N, 5.46%. ^{1}H NMR (400 MHz, $CDCl_3$, 298 K): δ 10.04 (d with broad ^{195}Pt satellites, J_{H-H} =5.2, 1H), 8.35 (d, J_{H-H} = 8.0 Hz, 1H), 7.80 (d, J_{H-H} = 8.7 Hz, 1H), 7.71-7.60 (m, 3H), 7.55 (d, J_{H-H} = 6.7 Hz, 4H), 7.32 (t, J_{H-H} = 7.7 Hz, 1H), 7.28-7.20 (m, 8H), 7.17-7.15 (m, 2H), 6.89 (dd, J_{H-H} = 7.2, J_{Pt-H} = 70 Hz, 1H), 6.15 (dd, J_{H-H} = 76.3, 15.5 Hz, 2H) ppm. MS ESI (*m*/*z*): 671.18 $[M-Br]^+$.

Synthesis of [Pt (N^C-ppy)(1,3-diethylbenzimidazol-2-yliden)Cl] (5)

The compound was prepared according to the procedure described for **2**using [Ag (1,3-diethylbenzimidazol-2-yliden)Br] (72 mg, 0.200 mmol) as starting material. Yield: 47 mg (56%)**.** Anal. Calcd for $C_{22}H_{22}ClN_3Pt$: C, 47.27; H, 3.97; N, 7.52. Found: C, 47.39; H, 3.97; N, 7.31%. ^{1}H NMR (300 MHz, $CDCl_3$, 298 K): δ 9.65 (d with broad ^{195}Pt satellites, J_{H-H} =5.6, 1H), 7.89 (t, J_{H-H} = 7.7 Hz, 1H), 7.78 (d, J_{H-H} = 8.0 Hz, 1H), 7.58 (d, J_{H-H} = 7.7 Hz, 1H), 7.54-7.45 (m, 1H), 7.4-7.3 (m, 3H), 7.08 (t, J_{H-H} = 7.5 Hz, 1H), 6.85 (t, J_{H-H} = 7.4 Hz, 1H), 6.39 (dd, J_{H-H} = 7.5, J_{Pt-H} = 72 Hz, 1H), 4.78 (q, J_{H-H} = 7.2 Hz, 4H), 1.54 (t, J_{H-H} = 7.3 Hz, 6H) ppm. MS ESI (*m*/*z*): 523.15 $[M-Cl]^+$, 582.10 $[M+Na]^+$, 1081.26 $[2M-Cl]^+$, 1140.21 $[2M+Na]^+$.

Synthesis of [Pt (N^C-ppy)(1,3-dibenzylimidazol-2-yliden)Cl] (6)

The compound was prepared according to the procedure described for **2** using [Ag (1,3-dibenzylimidazol-2-yliden)Br] (87 mg, 0.200 mmol) as starting material. Yield: 59 mg (62%)**.** Anal.Calcd for $C_{28}H_{24}ClN_3Pt$: C, 53.12; H, 3.82; N, 6.64. Found: C, 52.72; H, 3.92; N, 6.29%. ^{1}H NMR (300 MHz, $CDCl_3$, 298 K): δ 9.66 (d with broad ^{195}Pt satellites, J_{H-H} = 4.1, 1H), 7.87 (t, J_{H-H} = 7.1 Hz, 1H), 7.76 (d, J_{H-H} = 7.9 Hz, 1H), 7.58 (d, J_{H-H} =7.1 Hz, 1H), 7.44 (d, J_{H-H} = 5.9 Hz, 4H), 7.37-7.29 (m, 7H), 7.13 (t, J = 7.3 Hz, 1H), 6.99 (t, J = 7.0 Hz, 1H), 6.80 (s, 2H), 6.62 (dd, J_{H-H} = 7.3, J_{Pt-H} = 70 Hz, 1H), 5.69 (m, J_{H-H} = 62.4, 14.6 Hz, 4H) ppm. MS ESI (*m*/*z*): 597.16 $[M-Cl]^+$, 672.10 $[M+K]^+$, 1230.29 $[2M-Cl]^+$.

Photophysical Measurements

The photophysical measurements in solution were carried out using CH_2Cl_2, which was distilled prior to use. All solutions were carefully degassed before lifetime and quantum yield measurements when it was necessary. UV/Vis spectra were recorded with a LAMBDA 1050 spectrophotometer (Perkin Elmer) at concentrations 3×10^{-5} M (1 cm cuvettes). Emission spectra in solution were measured with a Fluorolog-3 (JY Horiba Inc.) spectrofluorimeter using concentrations ca. 3×10^{-5} M. The absolute emission quantum yield in solutions was determined by the comparative method using coumarin 102 in ethanol (Φ_r = 0.764)[19] as reference with the refraction indexes of dichloromethane and ethanol equal to 1.42 and 1.36 correspondingly. The following equation

$$\Phi_s = \Phi_r \frac{\eta_s^2 A_r I_s}{\eta_r^2 A_s I_r}$$

was used to calculate quantum yield, where Φ_s is the quantum yield of the sample, Φ_r is the quantum yield of the reference, η is the refractive index of the solvent, A_s and A_r are the absorbance of the sample and the reference at the wavelength of excitation, and I_s and I_r are the integrated areas of emission bands.[19]

Microcrystalline samples were used for the photophysical experiments in solid state. Steady-state photoluminescence spectra were recorded with a Fluorolog-3 spectrofluorimeter. Phosphorescence lifetimes were determined by TCSPC (Time-Correlated Single Photon Counting) method. The lifetime data were fit using the Jobin-Yvon software package and the Origin 8.1 program. Direct quantum yield measurements of the solid samples in KBr tablets were performed at room temperature with an integrating sphere from Quanta-phi.

DFT calculations

The structures of the ground (S_0) and first excited triplet (T_1) states of **1-6** were optimized using dispersion corrected density functional theory (DFT-D). The B97-1 exchange-correlation functional [20] in conjunction with the empirical dispersion scheme of Grimme [21] was used with the initial atomic coordinates determined by X-ray crystallography. A basis set comprising the 6-311G(d) basis set for the C, H, N, Cl atoms and the Stuttgart Relativistic Small Core [22,23] basis set for Pt and Br (for brevity this basis set is denoted as SRSC) was used. Vertical excitation energies for the ground state structure were computed using TDDFT calculations at the B97-1/SRSC level in order to evaluate the UV-Vis absorption spectrum. The $S_0 \leftarrow T_1$ phosphorescence emission energy was computed using TDDFT, TDDFT with the Tamm-Dancoff approximation[24] and within a ΔKohn-Sham DFT approach. All calculations were performed using the Q-Chem software package[25].

X-ray analysis

Crystals suitable for X-ray diffraction analysis were obtained by slow evaporation of dichloromethane from hexane/dichloromethane mixture. Crystal structures of **1-6** were determined by the means of single crystal X-ray diffraction analysis. Crystals were fixed on a micro mounts and the diffraction data had been collected on the different diffractometers. A crystal of **1** was placed on a Bruker Smart Apex II diffractometer and measured at a temperature of 210K using monochromated Mo*Kα* radiation. Crystals of **2, 5** and **6** were placed on a Agilent Technologies Excalibur Eos diffractometer and measured at a temperature of 100K using monochromated Mo*Kα* radiation. Crystal of **3** was placed on a Agilent Technologies SuperNova Atlas diffractometer and measured at a temperature of 100K using monochromated microfocused Cu*Kα* radiation. Crystal of **4** was placed on a Agilent Technologies SuperNova Atlas diffractometer and measured at a temperature of 100K using monochromated microfocused Mo*Kα* radiation. The unit cell parameters and refinement characteristics for the crystal structures of **1-6** are given in the Table 1. The structures had been solved by the direct methods and refined by means of the SHELXL–97 program [26] incorporated in the *OLEX2* program package [27]. The carbon-bound H atoms were placed in calculated positions and were included in the refinement in the 'riding' model approximation, with U_{iso}(H) set to 1.5U_{eq}(C) and C–H 0.96 Å for the CH_3 groups, U_{iso}(H) set to 1.2U_{eq}(C) and C–H 0.97 Å for the CH_2 groups and U_{iso}(H) set to 1.2U_{eq}(C) and C–H 0.93 Å for the CH groups. Absorption correction for **1** was applied using SADABS program[28]. Empirical absorption correction for **2-6** was applied in CrysAlisPro program complex[29] using spherical harmonics, implemented in SCALE3 ABSPACK scaling algorithm. Supplementary crystallographic data for this paper have been deposited at Cambridge

Crystallographic Data Centre (CCDC 985315-985316 for **1-2** and CCDC 985306-985309, for **3-6**) and can be obtained free of charge via www.ccdc.cam.ac.uk/data_request/cif.

Table 1 X-ray crystallographic data of **1-6**.

Compound	**1**	**2**	**3**	**4**	**5**	**6**
Formula	$C_{32}H_{26}BrN_3Pt$	$C_{32}H_{26}ClN_3Pt$	$C_{41}H_{33}Cl_2N_3Pt$	$C_{34}H_{26}BrN_3Pt$	$C_{22}H_{22}ClN_3Pt$	$C_{28}H_{24}ClN_3Pt$
Crystal System	Monoclinic	Monoclinic	Monoclinic	Monoclinic	Monoclinic	Monoclinic
a (Å)	11.3481(7)	11.2555(2)	10.03668(10)	11.1357(3)	11.4645(2)	11.2550(2)
b (Å)	16.8174(11)	16.6139(2)	32.6946(2)	17.1603(4)	10.03648(15)	14.2139(3)
c (Å)	14.9469(10)	14.7861(3)	11.23058(11)	14.9407(4)	18.1023(3)	15.1471(4)
α (°)	90	90	90	90	90	90
β (°)	106.5640(10)	107.167(3)	112.9906(11)	105.474(3)	103.2305(16)	106.113(2)
γ (°)	90	90	90	90	90	90
V (Å^3)	2734.2(3)	2641.79(10)	3392.53(5)	2751.54(12)	2027.62(6)	2327.98(9)
Molecular weight	727.56	683.10	833.69	751.58	558.97	633.04
Space group	$P2_1/n$	$P2_1/n$	$P2_1/c$	$P2_1/n$	$P2_1/n$	$P2_1/n$
μ (mm^{-1})	6.619	5.439	9.445	6.580	7.063	6.164
Temperature (K)	210(2)	100(2)	100(2)	100(2)	100(2)	100(2)
Z	4	4	4	4	2	4
D_{calc} (g/cm^3)	1.767	1.717	1.632	1.814	1.831	1.806
Crystal size (mm^3)	0.35 × 0.20 × 0.15	0.27 × 0.21 × 0.14	0.28 × 0.22 × 0.12	0.16 × 0.14 × 0.12	0.18 × 0.15 × 0.10	0.20 × 0.18 × 0.13
Radiation	Mo$K\alpha$	Mo$K\alpha$	Cu$K\alpha$	Mo$K\alpha$	Mo$K\alpha$	Mo$K\alpha$
Total reflections	21735	13173	54992	17261	18761	11999
Unique reflections	4815	5843	7133	6296	6211	5344
Angle range 2θ (°)	3.74–50.00	5.69–54.99	8.98–153.40	6.08–57.00	5.46–62.00	5.28–55.00
Reflections with $\|F_o\| \geq 4\sigma_F$	3505	4600	6945	5774	5661	4363
R_{int}	0.0521	0.0417	0.0319	0.0253	0.0322	0.0298
R_σ	0.0479	0.0643	0.0151	0.0311	0.0299	0.0435
R_1 ($\|F_o\| \geq 4\sigma_F$)	0.0328	0.0345	0.0407	0.0380	0.0265	0.0270
wR_2 ($\|F_o\| \geq 4\sigma_F$)	0.0886	0.0571	0.0910	0.1626	0.0666	0.0532
R_1 (all data)	0.0490	0.0523	0.0417	0.0428	0.0301	0.0408
wR_2 (all data)	0.0932	0.0647	0.0915	0.1682	0.0691	0.0580
S	0.956	1.051	1.104	0.976	1.064	1.065
ρ_{min}, ρ_{max}, e/Å^3	–1.579, 0.635	–1.018, 1.537	–2.643, 2.164	–1.827, 0.890	–1.791, 3.032	–0.890, 2.014

$R_1 = \Sigma||F_o| - |F_c||/\Sigma|F_o|$; $wR_2 = \{\Sigma[w(F_o^2 - F_c^2)^2]/\Sigma[w(F_o^2)^2]\}^{1/2}$; $w = 1/[\sigma^2(F_o^2)+(aP)^2 + bP]$, where $P = (F_o^2 + 2F_c^2)/3$; $s = \{\Sigma[w(F_o^2 - F_c^2)]/(n - p)\}^{1/2}$ where n is the number of reflections and p is the number of refinement parameters.

OLED device fabrication and measurements

The studied devices with the structure ITO/PEDOT:PSS/PVK:**complex**/BATH/AlQ_3/Yb consist of poly(3,4-ethylenedioxythiophene)-poly(styrenesulfonate) (PEDOT:PSS) as a hole injection layer, emissive complex doped into poly(9-vinylcarbazole) (PVK), 4,7-diphenyl-1,10-phenanthroline (BATH) as a hole-blocking layer and tris(8-hydroxyquinoline)aluminum (AlQ_3) as an electron-transporting layer. The devices were fabricated by spin-coating and vacuum deposition. A commercial ITO on a glass substrate with 5 $\Omega\ \varepsilon^{-1}$ was used as the anode material (Luminescence Technology Corp.) and commercial Yb, 99.9% trace metal basis, (Sigma-Aldrich) as the cathode material. ITO glass was sonicated in acetone, isopropanol and deionized water for 10 min at 60 °C followed by grying at 120 °C for 30 min. Substrates was treated in a UV ozone cleaner for 10 min to improve the working potential of the anode electrode. PEDOT:PSS layer was spin-coated onto ITO substrates from a 5 wt.% dispersion in water at 4000 rpm for 30 s. The substrates were thereafter annealed at 120 °C for 10 min to remove any residual water. Pt(II) complexes (10 wt%) and the PVK polymer host were dissolved in chloroform. The solutions were spin-cast at 3000 rpm for 30 s and baked at 80 °C for 1 h. The substrates were then loaded into the vacuum deposition chamber. The thickness of emissive layers was determined by ellipsometry.BATH, AlQ_3, and Yb were deposited onto the ITO glass by thermal deposition at 1×10^{-6} Torr pressure. The deposition rate for the organic compounds and Yb complex was 1 nm/s. The thickness of the vacuum deposited layers was determined using calibrated quartz resonator. The active area of the devices was 5×5 mm. The EL spectra in the visible region and current–luminance–voltage characteristics were measured with an Ocean Optics USB2000 fluorimeter calibrated with an Ocean Optics LS-1 CAL lamp, the computer controlled GWInstek PPE-3323 power supply and a GW Instek GDM-8246 digital multimeter. The device characteristics were measured under ambient conditions.

Results and Discussion

A series of cyclometallated Pt(II) complexes **1-6** (Fig. 1) containing NHC ligands was synthesized according to the Scheme 1 in moderate to good yield.

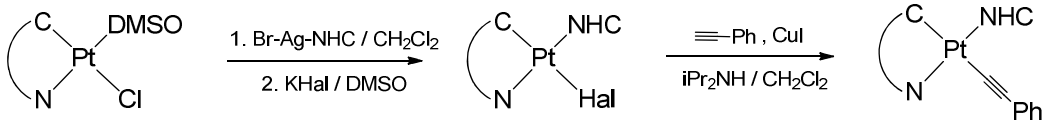

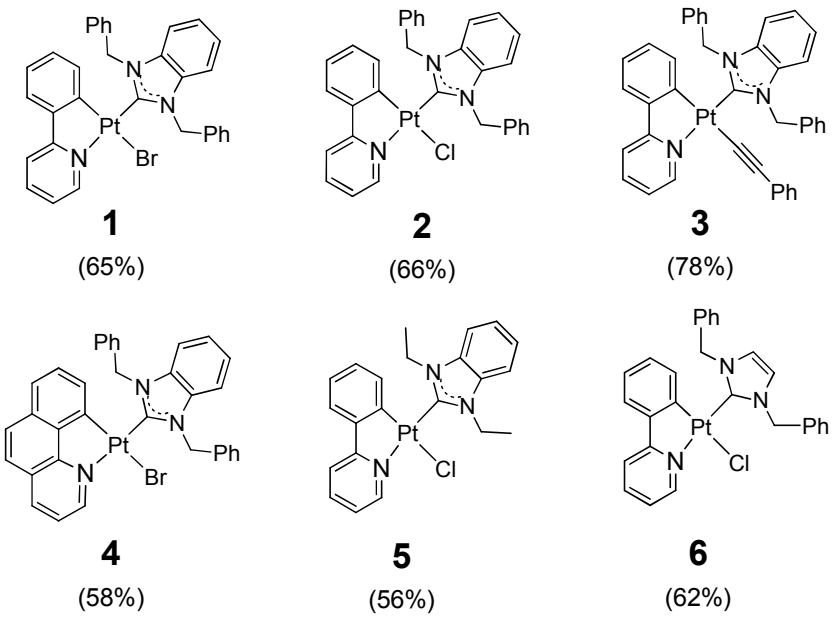

Scheme 1. Synthesis and schematic structure of the complexes **1-6**.

Solid state structure of the compounds obtained (**1-6**) was determined using single crystal X-ray crystallography. Two representative structures are shown in Figs. 1 and 2, selected structural parameters are given in figure captions. Structures of the other compounds are shown in Fig. S1 (see Supporting Information†).

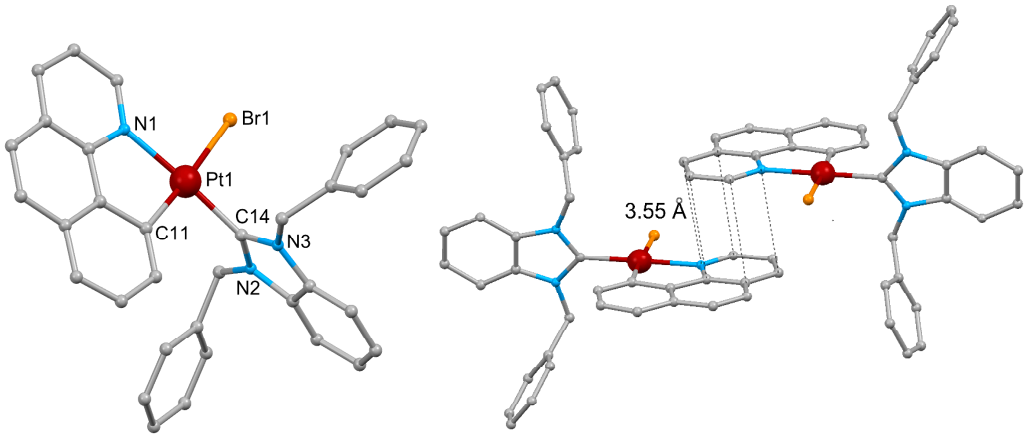

Fig. 1. Solid state structure of **4**. Left part of the figure shows intermolecular contacts in the crystal cell. Selected bond distances (Å): Pt1–C11 2.027(7), Pt1–C14 1.985(7), Pt1–N1 2.088(5), Pt1–Br1 2.4844(8). Selected angles (˚): C11–Pt1–Br1 176.2(2), C14–Pt1–Br1 92.2(2), C11–Pt1–C14 91.5(3), N1–Pt1–Br1 93.1(2), C11–Pt1–N1 83.2(3), C11–Pt1–C12–N3 73.9(6).

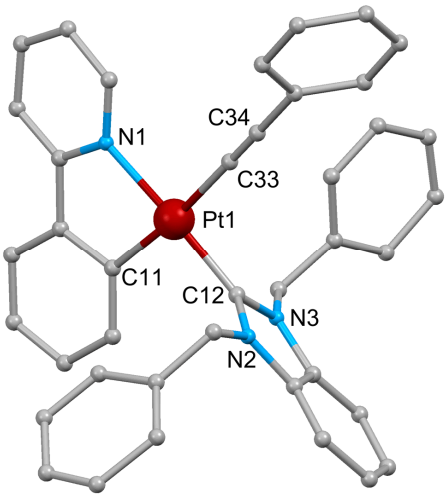

Fig. 2. Solid state structure of **3**. Selected bond distances (Å): Pt1–C11 2.031(4), Pt1–C12 1.967(4), Pt1–N1 2.078(3), Pt1–C33 2.104(4), C33-C34 1.120(5). Selected angles (°): C11–Pt1–C33 174.2(2), C12–Pt1–C33 92.2(2), C11–Pt1–C12 93.2(2), N1–Pt1–C33 94.6(1), C11–Pt1–N1 80.2(1), C11–Pt1–C12–N3 67.4(4).

All the complexes display a square-planar geometry with the phenylpyridine and benzoquinoline ligands coordinated in a chelate manner to form five-membered metallocycles. The NHC ligand occupies *trans* position with respect to the nitrogen atom of the metallocycle whereas the halide or alkynyl ligands are *cis* relative to the nitrogen atom of cyclometallated ligand. All the distances between the platinum center and coordinated atoms fall in the range typical for the compounds of this sort. The angular parameters of the platinum environment also do not display significant deviations from the square-planar geometry. The plane of the five-membered NHC ring is somewhat twisted relative to the platinum centered quadrangle to fit the ring substituents into the crystal cell. It has also to be noted that in contrast to the other compounds studied the benzoquinoline complex **4** displays a π-stacking interaction in the crystal cell to form π–bound dimers with a typical distance of ca. 3.5 Å between stacked aromatic rings, as shown in Fig. 2. This is evidently determined by the extended aromatic system of the ligand that make possible to avoid steric hindrance upon packing of the molecules in the crystal cell. Formation of the dimeric aggregates has a considerable impact onto photophysical characteristics of **4**, *vide infra*.

In solution, the complexes **1-6** were characterized using the ESI^+ mass spectrometry and ^1H NMR spectroscopy. The mass spectra of all complexes (Figs. S11-S17†) display positive ions generated either by dissociation of halide (alkynyl) ligands or by association of the complex molecule with Na^+ (K^+) ions. This observation clearly indicates that the stoichiometry found in solid state is retained in solution. The 1D ^1H and ^1H-^1H COSY NMR spectra of **1-6** (Figs. S2-S10†) are completely compatible with the stoichiometry and square-planar structure of these compounds shown in Figs. 1, 2 and S1. The number, multiplicity and relative positions of the

signals observed (see Experimental and Figs. S2-S10†) are consistent with the coordination mode of the ligands revealed in solid state and the general structural motif of the square-planar complexes.

Photophysical properties

The complexes studied are luminescent both in solution and in solid state. Absorption and emission spectra of **1-6** in dichloromethane solution are shown in Fig. 3, spectroscopic parameters and photophysical data obtained in solution and in solid state are summarized in Tables 2 and 3, respectively.

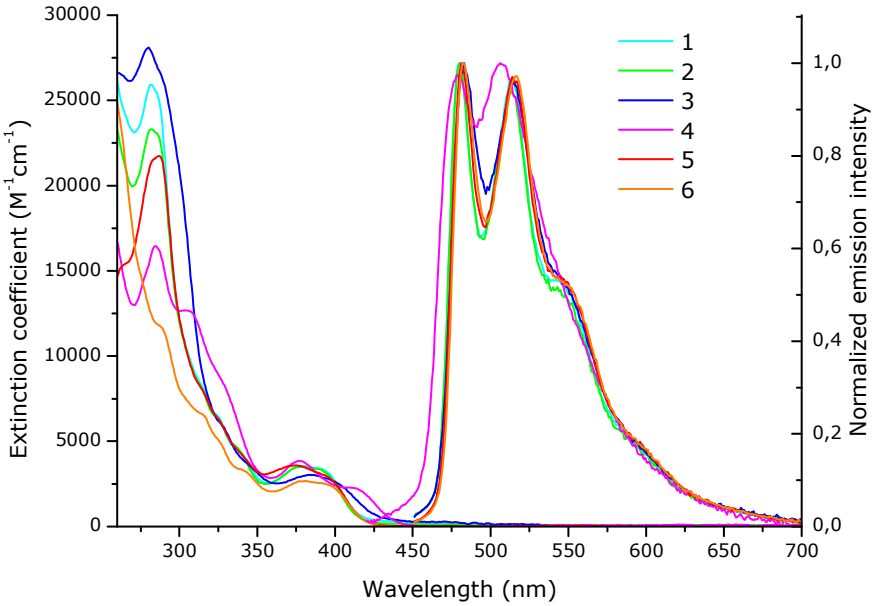

Fig. 1. Room temperature absorption and emission (λ_{ex} 385 nm) spectra of **1-6** in dichloromethane solution.

Table 2. Photophysical properties of **1–6** in dichloromethane solution (λ_{ex} = 385 nm).

	λ_{abs}, nm (ε*10^{-3} , M^{-1} cm^{-1})	λ_{em}, nm	λ_{ex}, nm	$\tau_{aer}/\tau_{deg}^{*}$, μs	$\Phi_{aer}/\Phi_{deg}^{*}$, %
1	282 (26), 323sh (7), 335sh (5), 377 (4)	480, 515, 545sh, 590sh	335sh, 380	0.17/1.04	0.6/2.3
2	282 (23), 324sh (6), 335sh (5), 378 (3)	480, 515, 545sh, 590sh	335sh, 380	0.12/1.00	1.0/5.4
3	280 (28), 325sh (6), 343sh (4), 384 (3)	480, 515, 545sh, 590sh	340sh, 387	0.11/0.20	0.5/1.3
4	284 (16), 305sh (13), 323sh (9), 377 (4), 411sh (2)	478, 506	304, 325sh, 399	0.23/1.41	<0.1/0.3
5	287 (22), 325sh (6), 338sh (4), 375 (4)	480, 515, 545sh, 590sh	335sh, 385	0.25/1.50	1.1/7.9
6	287sh (12), 312sh (7), 336sh (3), 380 (3)	480, 515, 545sh, 590sh	338sh, 385	0.23/1.22	1.1/7.4

* aer/deg, measurements made in aerated/degassed solutions.

Table 3. Photophysical data for complexes **1–6** in solid state.

	λ_{em},nm[1]	λ_{ex},nm [1]	τ, μs [1]	Φ, % [2]
1	481, 505sh, 512, 540, 580sh	442, 473	0.69 (55%) 2.22 (45%)	15.8
2	482, 505sh, 512, 540, 580sh	442, 473	0.64 (45%) 2.29 (55%)	16.0
3	495sh, 514, 540sh, 580sh	442, 474	0.98 (42%) 4.04 (58%)	14.2
4	490sh, 517, 558	408, 460sh	4.75 (31%) 13.62 (69%)	
5	486, 516, 545sh, 595sh	445, 475	0.34 (60%) 0.90 (40%)	2.7
6	479, 493, 512, 540sh, 580sh	443, 477	1.33 (34%) 3.79 (66%)	9.4

[1] measurements made using powder samples

[2] measurements made using the powder grounded and pressed into KBr pellet

In solution the complexes display strong high energy absorption in the 280-310 nm range which can be assigned to intraligand electronic transitions whereas weak absorption bands in the 380-410 nm interval originate from MLCT transitions typical for cyclometallated square-planar Pt(II) complexes.[3,4,30] Photoexcitation of the complexes **1-6** in degassed CH_2Cl_2 solution gives green emission with the quantum yield ranging from 0.3 to 8%. Large Stokes shift together with the lifetime values in the microsecond domain are indicative of emission origin from the triplet manifold. The triplet nature of the emissive excited state is evidently determined by strong spin-orbit coupling to the central metal atom. The emission bands display clearly resolved vibrational spacing, ca. 1400 cm^{-1} for **1-3, 5** and **6**, whereas emission band of **4** displays substantially lower spacing of 1150 cm^{-1}. The former value fits well vibrational frequencies of phenylpyridine and clearly points to strong involvement of the aromatic system into emissive excited state, whereas

the latter might be explained by the difference in vibrational frequencies of the benzoquinoline aromatic systems involved into emissive transitions. Analogously to the previously studied Pt(II) complexes[3,4,30] this emission may be mostly determined by the mixed ^{3}IL($\pi\rightarrow\pi^*$)/^{3}MLCT($d\pi\rightarrow\pi^*$) transitions with substantial prevalence of the former one. It is also worth noting that the shape of the emission bands as well excitation spectra for the complexes containing phenylpyridine (**1-3, 5, 6)**, see Fig. 3, are nearly identical and essentially differ of those for the complex **4** containing the benzoquinoline ligand that indicates once more a primary contribution of the cyclometallated ligands into IL and MLCT transitions. Analysis of the data obtained also shows that in degassed solutions quantum yield of emission as well as excited state lifetime for the phenylpyridine complexes (**1-3, 5, 6**) display appreciable correlation with the Pt-C(cyclometallated) bond length (see Table S1 and Fig. S17) that is completely in line with the trend observed earlier[31] for the photophysics of structurally related Pt(II) complexes. The lower values of the Pt-C bond length bond (stronger ligand field effect) results in higher energy of the d-d excited state thus cutting off nonradiative relaxation through this excited state. In aerated solutions emission intensity drops ca. order of magnitude that clearly points to effective luminescence quenching by molecular oxygen that is typical for triplet emission from unshielded chromophoric center of the platinum(II) complexes.

In solid state all but one complexes display luminescence with the shape of emission bands essentially similar to those observed in solution (Fig. S21) that points to similarity of the energy of emissive transitions in both phases. The only exception is complex **4**, which shows a slight red shift of emission maximum and longer/broader band tail in the 600-800 nm range. This again may be ascribed to the π-stacking of the benzoquinoline ligand that strongly affects specific features of the complex emission compared to the rest of the complexes studied.

It is worth noting that the emissive excited states in solid state display a double exponential decay (Table 3) that indicates the presence of different conformers in the crystal cell, which have similar energy characteristics but differ in the vibrational relaxation pathways. The excited state lifetimes fall in the microsecond domain that indicates triplet origin of the emission for all but one (**5**) complex the lifetime values are substantially higher compared to the values obtained in solution. This observation points to considerable contribution of vibrational non-radiative deactivation of the triplet excited state in solution, which is suppressed in solid state by rigid packing of the molecules in crystal cell as well as by the absence of emission quenching through interaction with solvent molecules.

Computational Studies

The main structural parameters, namely the bond distances and angles around the Pt center, calculated for the S_0 and T_1 states of the complexes **1-6** together with the values for the S_0 state derived from X-ray studies are shown in Table 3. For the S_0 state, there is good agreement between the DFT optimized and X-ray structures. The average deviation between experiment and theory in the bond lengths and bond angles is within 0.03 Å and 1^{o}, respectively. The highest occupied molecular orbital (HOMO) and lowest unoccupied molecular orbital (LUMO) for the complexes are depicted in Figure 4. This shows there is no qualitative change in the nature of these orbitals for the different complexes. The HOMO can be described as an out of phase combination of a Pt d orbital with the π or p orbitals associated with X (where X=Cl, Br or -≡-Ph) and the π orbitals of the ring coordinated opposite to X. The LUMO has little contribution from the Pt atom and can be described as a π* orbital that is localized on the phenylpyridine group. In the T_1 state these two orbitals are singly occupied, and the corresponding structural parameters for the T_1 state are also given in Table 3. Comparison of the S_0 and T_1 structures shows a decrease in the Pt-N, Pt-C_{cycl} and Pt-X bond lengths on the formation of the T_1 state, while the majority of the structures show an increase or no change in the Pt-C_{NHC} bond length. The HOMO is clearly antibonding along the Pt-X and Pt-C_{cycl} bonds, which is consistent with a shortening of these bonds on the formation of the T_1 state.

Table 3. Comparison between DFT optimized structures for the S_o and T_1 states and the experimental (X-ray crystallography) structures for the S_o state. Bond distances in Å and angles in degrees.

	1			**2**			**3**		
	X-ray	S_0	T_1	X-ray	S_0	T_1	X-ray	S_0	T_1
Pt-N	2.09	2.09	2.06	2.08	2.07	2.04	2.08	2.06	2.04
Pt-C_{cycl}	2.00	1.96	1.93	1.98	1.96	1.92	2.03	2.02	1.97
Pt-C_{NHC}	1.95	1.92	1.94	1.96	1.96	1.94	1.97	1.92	1.94
Pt-X	2.47	2.52	2.52	2.39	2.45	2.44	2.10	1.99	1.97
X-Pt-C_{NHC}	90.4	88.9	88.1	90.6	89.6	88.5	92.2	88.3	88.3
C_{NHC}-Pt-C_{cycl}	93.7	93.9	93.8	94.6	93.5	93.5	93.2	95.1	94.2
C_{cycl}-Pt -N	81.8	81.4	82.9	80.8	81.8	83.3	80.2	81.0	82.5
N-Pt-X	94.1	95.8	95.3	94.0	95.1	94.7	94.6	95.7	95.1
	4			**5**			**6**		
	X-ray	S_0	T_1	X-ray	S_0	T_1	X-ray	S_0	T_1
Pt-N	2.09	2.10	2.07	2.07	2.07	2.04	2.07	2.07	2.04
Pt-C_{cycl}	2.03	1.97	1.92	1.98	1.96	1.92	1.99	1.96	1.92
Pt-C_{NHC}	1.99	1.91	1.94	1.96	1.92	1.92	1.97	1.94	1.95
Pt-X	2.48	2.52	2.50	2.40	2.45	2.44	2.40	2.45	2.44
X-Pt-C_{NHC}	92.2	90.1	89.7	89.3	89.1	87.8	90.0	89.1	88.3
C_{NHC}-Pt-C_{cycl}	91.5	92.9	92.8	94.2	94.5	94.7	94.4	94.5	94.4
C_{cycl}-Pt -N	83.2	82.1	83.3	81.4	81.6	83.2	80.8	81.7	83.3
N-Pt-X	93.1	94.9	94.3	95.1	94.8	94.3	94.7	94.7	94.1

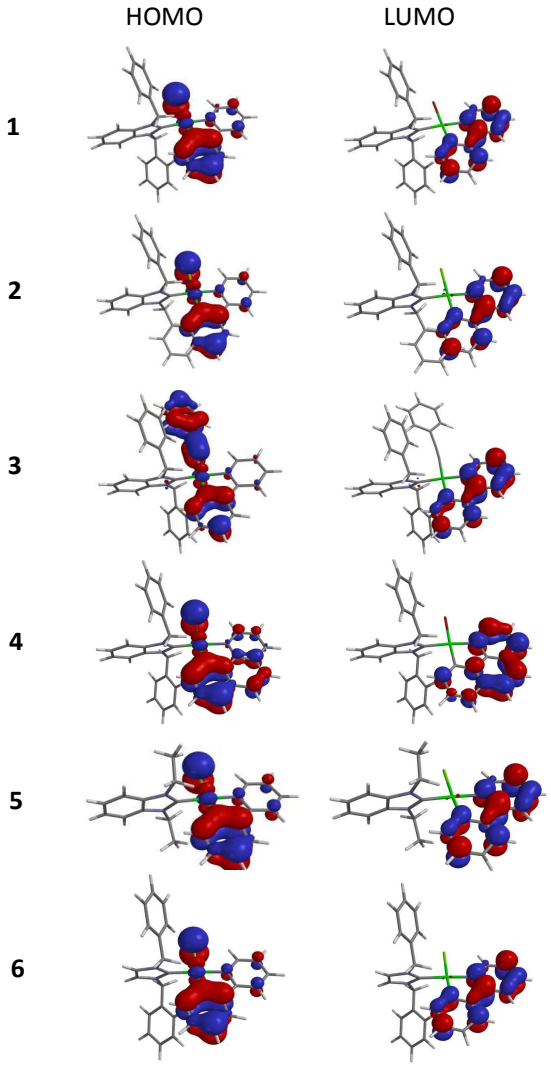

Fig. 4. Kohn-Sham HOMO and LUMO for the S_o states of complexes **1-6**.

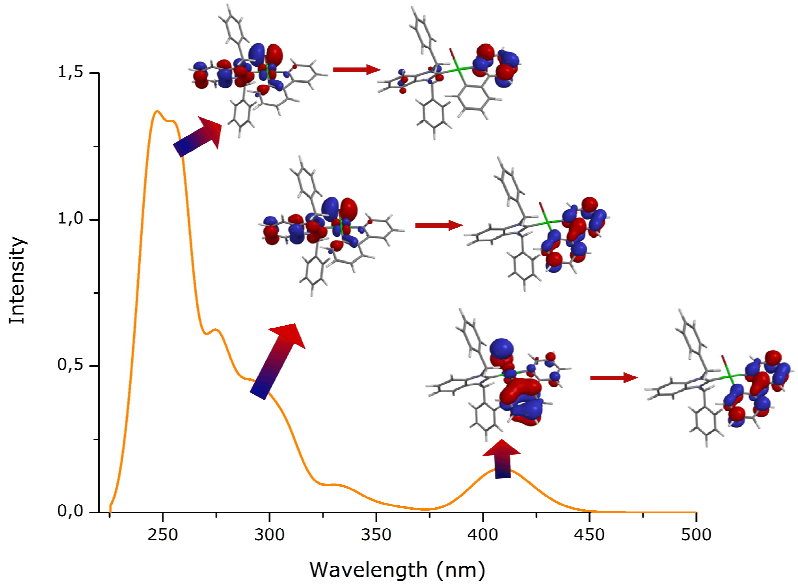

Fig. 5. Computed TDDFT/SRSC absorption spectrum with orbitals illustrating the major transitions for complex **5**.

Fig. 5 shows the computed TDDFT/SRSC spectrum for complex **5**. The calculations predict bands at 408, 293 with a shoulder at 275 and 250 nm, which compares to bands observed in experiment at 375, 325 and 287 nm. This difference between experiment and the calculations lies within the typical error that is associated with TDDFT calculations particularly considering the experimental spectrum is measured in CH_2Cl_2 while the calculations correspond to the gas phase. This indicates that the hybrid functional B97-1 provides an adequate description of these transitions. The lowest energy band at about 400 nm arises from excitation from the HOMO, which is a mixture of Pt d and ligand p and π orbitals, to the LUMO which is a ligand π* orbital. Consequently this transition can be described as a mixture of MLCT d→π* and intra-ligand π→π* character. The band at 300 nm arises predominantly from excitation from two occupied orbitals of lower energy than the LUMO. These orbitals are largely comprised of ligand π orbitals, although there remains a small contribution from the Pt d orbitals.

Similarly, the most intense band corresponds to an excitation π to π* orbitals associated with the ligands. As such, these finding are consistent with the description of the broad feature at 225-325 nm as arising from intra-ligand π→π* transitions in previous studies. Although we note that there remains a small component of MLCT character in these transitions. Computed spectra for all six complexes are shown in Figure 6 with the band positions given in Table 4. For all of

the complexes, a weaker band is predicted at approximately 400 nm with broad features between 225 and 350 nm.

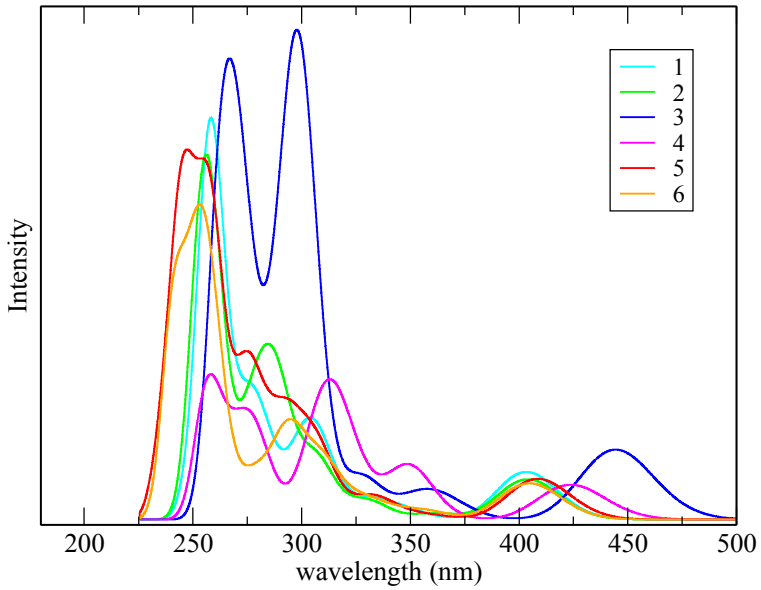

Fig. 6. Computed TDDFT/SRSC absorption spectra for the complexes **1-6**.

Table 4. Summary of the wavelengths of the predicted absorption bands ($\lambda_{abs.}$) from the TDDFT calculations and wavelengths of emission (λ_{em}).

Complex	$\lambda_{abs.}$, nm	λ_{em}, nm		
		TDDFT	TDDFT/TDA	ΔKohn-Sham
1	258, 275 sh, 304, 403	588	559	552
2	256, 284, 306 sh, 332 sh, 404	577	550	554
3	267, 298, 329 sh, 359 sh, 445	595	577	537
4	258, 274, 313, 349, 424	548	537	516
5	250, 293, 275 sh, 408	587	559	545
6	253, 295, 405	587	558	547

The experimental emission spectra for all compounds except **4** are very similar and show a broad band with peaks at 485 and 515 nm. The spectrum for **4** has a similar shape but is shifted to a lower wavelength. Table 5 gives the computed $S_0 \leftarrow T_1$ transition energies using various DFT based approaches. This transition has a similar character to the feature at about 400 nm in the absorption spectra. The predicted TDDFT transition energies are consistently higher in energy than the values observed in experiment, while TDDFT in combination with the TDA gives energies closer to experiment. This error is associated with the triplet instability in TDDFT and

is consistent with recent work[32] demonstrating that the TDA significantly improves the calculated transition energies for this type of transition. The problems associated with triplet instability are avoided in a ΔKohn-Sham approach, and the transition energies predicted with this method are in reasonable agreement with the TDDFT/TDA values and the closest to experiment. Focusing on the ΔKohn-Sham results, the predicted emission wavelengths are similar for complexes **1**, **2**, **5** and **6** with a lower wavelength predicted for complex **4**. This is consistent with shift in the emission band observed in the experimental measurements. Comparison of the structures suggests that this change is a consequence of coordination to the benzoquinoline ligand compared to phenylpyridine. The orbitals associated with this ligand are involved in the relevant orbitals for the transition, and it is interesting to note that this change in ligands has a greater effect on the emission than changing Cl to Br. For complex **3** there is a slight inconsistency with experiment, where the calculations predict a change in the emission energy compared to **1**, **2**, **5** and **6**. While the structure of **3** is different from the other complexes, and hence a change in emission energy might be expected, there is no evidence for this in the experimental measurements.

Electroluminescent properties

Encouraged by the results of photoluminescence (PL) displayed by the compounds **1-6** we studied the electroluminescent (EL) properties of these complexes. For this purpose multilayer doped OLED devices **A-F** with the structure ITO/PEDOT:PSS (30 nm)/PVK:**complex** (10 wt.%, 50 nm)/BATH (15 nm)/AlQ_3 (25 nm)/Yb (150 nm) were fabricated. The OLEDs exhibited green emission with similar CIE coordinates for devices **A-C, E** and **F**, while coordinates for **D** are slightly different (Fig. S23). With the exception of **4**, which revealed broad-band emission with the maxima at 503 nm, the EL spectra of the complexes consist of two overlapped but rather defined peaks (Fig. 7), which are red-shifted by 5-10 nm relative to PL of the corresponding compounds. Obviously, the EL of all compounds can be attributed to emission from mixed ^{3}IL/^{3}MLCT excited state. It should be noted that undesirable luminescence originating from PVK host as well as AlQ_3 was not detected. The absence of PVK band at 440 nm is reasonable evidence of good quantum confinement and successful energy transfer from $^3T_{1p}$ and $^3T_{1f}$ excited states of PVK[33] to mixed ^{3}IL/^{3}MLCT state of the platinum(II) complex in the studied host-guest system. It should be noted however that efficiency of the devices based on triplet host materials such as PVK and CBP can dramatically decrease with increasing applied electrical field due to triplet-triplet (T-T) annihilation in the matrix.[34,35]

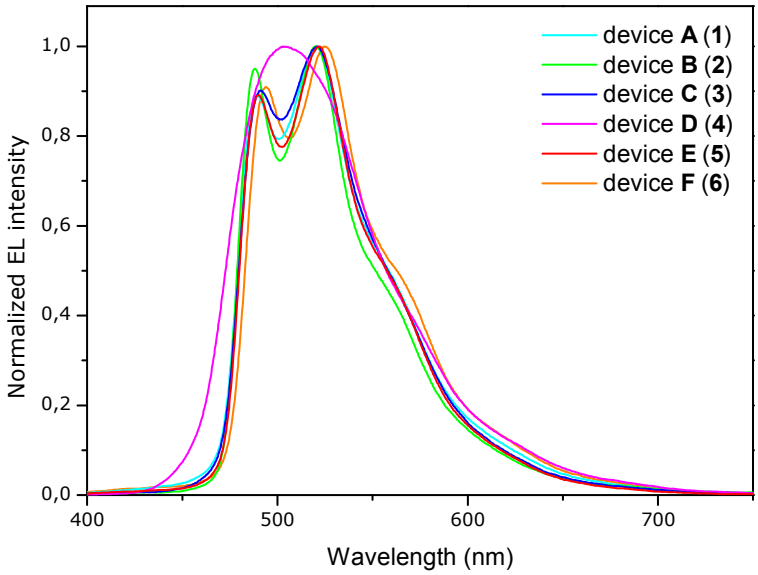

Fig. 7. Electroluminescence of the **A**-**F** devices.

The turn-on voltages for the devices were in the range of 6 to 6.5 V. The maximum brightness of 1896 cd/m^2 was achieved at 20 V for the device **B** comprised of **2** as luminescent dopant. Moreover, for this complex the highest values of efficiencies among full series of synthesized compounds were obtained: $\eta_{c\ max}$=3.18 cd/A, $\eta_{p\ max}$=0.9 lm/W and EQE_{max}=3.2 %. Current-luminance-voltage characteristics and performance data for the fabricated OLEDs are presented in Fig. 8 and in Table 5, respectively. Their current and power efficiency are presented in Figs. S24 and S25.

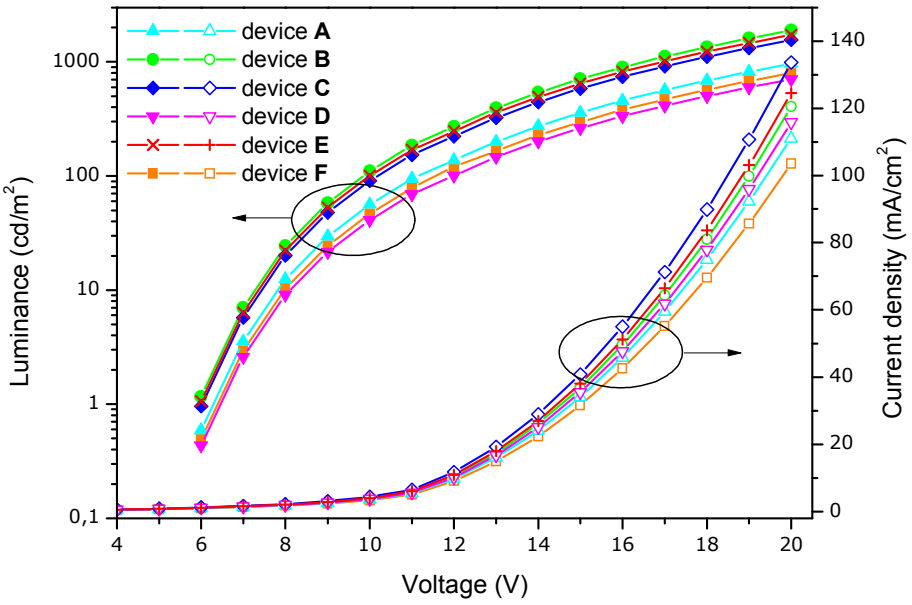

Fig. 8. Current-luminance-voltage relationship for the **A-F** devices.

Table 5. Performance data for devices **A-F**

Device	V_0 [a] (V)	λ_{max} (nm)	L_{max} [b] (cd/m^2)	$\eta_{c\ max}$ [c] (cd/A)	$\eta_{c\ max}$ [d] (lm/W)	EQE_{max} [e] (%)	CIE 1931 [f] (x, y)
A	6.5	489, 521	963	1.75	0.5	2.1	0.219, 0.664
B	6	488, 520	1896	3.18	0.9	3.2	0.202, 0.686
C	6	491, 521	1561	2.36	0.67	2.9	0.210, 0.674
D	6.5	503	705	1.23	0.35	1.6	0.223, 0.578
E	6	490, 522	1729	2.81	0.8	3.0	0.208, 0.685
F	6.5	494, 525	802	1.56	0.44	1.8	0.236, 0.676

[a] Turn-on voltage (at 1 cd/m^2). [b] Maximum luminance (at 20 V). [c] Maximum current efficiency. [d] Maximum power efficiency. [e] Maximum external quantum efficiency. [f] CIE chromaticity coordinates.

It is well known that EL device efficiency depends considerably on the method of fabrication and device structure. In order to estimate the performances of prepared devices a comparison with the other solution-processed OLEDs based on PVK:Pt(II)-complex emissive layer has been done. In the vast majority of publications it was demonstrated, that cyclometalated Pt(II) compounds incorporated into PVK matrix reveal poor to moderate EL characteristics.[36–40] The best results, which are similar to those presented above, were achieved for the series of Pt(II) complexes bearing tridentate 3-[6'-(naphthalene-2''-yl)pyridine-2'-yl]isoquinoline ligands with fluorine substituents reported by Yuen et al.[41] We believe that efficiencies of studied OLEDs can be improved by optimization of the concentration of luminescent complex and developing of more appropriate host-guest system. This study is now in progress.

Conclusion

A series of N-heterocyclic carbene Pt(II) complexes based on cyclometallated phenylpyridine and benzoquinoline ligands has been synthesized and structurally characterized in solid state and in solution to show typical square planar geometry with the NHC ligand in trans position with respect to the nitrogen atom of the cyclometallated ligand. The complexes display moderate to strong phosphorescence in solution and in solid state, which are related to metal center modulated intraligand π–π* transitions located at aromatic system of cyclometallated ligands with some contribution of MLCT excited state. This conclusion is strongly supported by the difference in photophysical data found for the phenylpyridine and benzoquinoline complexes and essentially identical characteristics revealed for the phenylpyridine compounds, in spite of substantial variations in the composition of the lateral ligand environment. The correlation between Pt-C(cyclometallated) bond length and emission Q.Y./excited state lifetime for the phenylpyridine complexes also indicates primary contribution of the π–π* excited state localized onto cyclometallated ligands in the emission observed. These observations point to possible ways of Q.Y. augmentation through the variation in the composition of ligand sphere, which could give rise to stronger ligand field effect in the Pt-C bonding. The nature of emission observed was also studied using DFT and TDDFT approach which confirmed assignment mentioned above. The compounds obtained were also used to prepare OLED devices, which display good luminance efficiency emitting in green area of the visible spectrum.

Acknowledgements

The authors appreciate financial support from the St. Petersburg State University research grant 0.37.169.2014, and RFBR grant 13-03-12411. The NMR, photophysical, analytical and crystallographic measurements were performed using core facilities of St. Petersburg State University Research Park: Center for Magnetic Resonance, Center for Optical and Laser Materials Research, Center Chemical Analysis and Materials Research and the X-ray Diffraction Centre, respectively. The computations were performed using the High Performance Computing (HPC) facility at the University of Nottingham. EB acknowledges an ERC Consolidator grant for financial support.

References

1. J. A. G. Williams, S. Develay, D. L. Rochester and L. Murphy, *Coord. Chem. Rev.*, 2008, **252**, 2596–2611.
2. A. K.-W. Chan, E. S.-H. Lam, A. Y.-Y. Tam, D. P.-K. Tsang, W. H. Lam, M.-Y. Chan, W.-T. Wong and V. W.-W. Yam, *Chem. – Eur. J.*, 2013, **19**, 13910–13924.
3. C. Li, S. Wang, Y. Huang, B. Zheng, Z. Tian, Y. Wen and F. Li, *Dalton Trans.*, 2013, **42**, 4059–4067.
4. A. Bossi, A. F. Rausch, M. J. Leitl, R. Czerwieniec, M. T. Whited, P. I. Djurovich, H. Yersin and M. E. Thompson, *Inorg. Chem.*, 2013, **52**, 12403–12415.
5. S. K. Yen, D. J. Young, H. V. Huynh, L. L. Koh and T. S. A. Hor, *Chem. Commun.*, 2009, 6831–6833.
6. J. J. Hu, S.-Q. Bai, H. H. Yeh, D. J. Young, Y. Chi and T. S. A. Hor, *Dalton Trans.*, 2011, **40**, 4402–4406.
7. K. Li, Y. Chen, W. Lu, N. Zhu and C.-M. Che, *Chem. – Eur. J.*, 2011, **17**, 4109–4112.
8. H. Uesugi, T. Tsukuda, K. Takao and T. Tsubomura, *Dalton Trans.*, 2013.
9. X. Yang, C. Yao and G. Zhou, *Platin. Met. Rev.*, 2013, **57**, 2–16.
10. C.-M. Che, M. Yang, K.-H. Wong, H.-L. Chan and W. Lam, *Chem. – Eur. J.*, 1999, **5**, 3350–3356.
11. D.-L. Ma, T. Y.-T. Shum, F. Zhang, C.-M. Che and M. Yang, *Chem. Commun.*, 2005, 4675–4677.
12. T. Zou, C.-N. Lok, Y. M. E. Fung and C.-M. Che, *Chem. Commun.*, 2013, **49**, 5423–5425.
13. J. R. Kumpfer, S. D. Taylor, W. B. Connick and S. J. Rowan, *J. Mater. Chem.*, 2012, **22**, 14196–14204.
14. N. Godbert, T. Pugliese, I. Aiello, A. Bellusci, A. Crispini and M. Ghedini, *Eur. J. Inorg. Chem.*, 2007, 5105–5111.
15. S. Patil, J. Claffey, A. Deally, M. Hogan, B. Gleeson, L. M. Menéndez Méndez, H. Müller-Bunz, F. Paradisi and M. Tacke, *Eur. J. Inorg. Chem.*, 2010, **2010**, 1020–1031.
16. J. A. V. Er, A. G. Tennyson, J. W. Kamplain, V. M. Lynch and C. W. Bielawski, *Eur. J. Inorg. Chem.*, 2009, **2009**, 1729–1738.
17. 20110257235, A1.
18. V. Gandin, M. Pellei, M. Marinelli, C. Marzano, A. Dolmella, M. Giorgetti and C. Santini, *J. Inorg. Biochem.*, 2013, **129**, 135–144.
19. K. Rurack and M. Spieles, *Anal. Chem.*, 2011, **83**, 1232–1242.
20. A. D. Becke, *J. Chem. Phys.*, 1993, **98**, 5648–5652.
21. S. Grimme, J. Antony, T. Schwabe and C. Mück-Lichtenfeld, *Org. Biomol. Chem.*, 2007, **5**, 741–758.
22. M. Kaupp, P. v R. Schleyer, H. Stoll and H. Preuss, *J. Chem. Phys.*, 1991, **94**, 1360–1366.
23. A. Bergner, M. Dolg, W. Küchle, H. Stoll and H. Preuß, *Mol. Phys.*, 1993, **80**, 1431–1441.
24. S. Hirata and M. Head-Gordon, *Chem. Phys. Lett.*, 1999, **314**, 291–299.
25. Y. Shao, L. F. Molnar, Y. Jung, J. Kussmann, C. Ochsenfeld, S. T. Brown, A. T. B. Gilbert, L. V. Slipchenko, S. V. Levchenko, D. P. O'Neill, R. A. D. Jr, R. C. Lochan, T. Wang, G. J. O. Beran, N. A. Besley, J. M. Herbert, C. Y. Lin, T. V. Voorhis, S. H. Chien, A. Sodt, R. P. Steele, V. A. Rassolov, P. E. Maslen, P. P. Korambath, R. D. Adamson, B. Austin, J. Baker, E. F. C. Byrd, H. Dachsel, R. J. Doerksen, A. Dreuw, B. D. Dunietz, A. D. Dutoi, T. R. Furlani, S. R. Gwaltney, A. Heyden, S. Hirata, C.-P. Hsu, G. Kedziora, R. Z. Khalliulin, P. Klunzinger, A. M. Lee, M. S. Lee, W. Liang, I. Lotan, N. Nair, B. Peters, E. I. Proynov, P. A. Pieniazek, Y. M. Rhee, J. Ritchie, E. Rosta, C. D. Sherrill, A. C. Simmonett, J. E. Subotnik, H. L. W. Iii, W. Zhang, A. T. Bell, A. K. Chakraborty, D. M. Chipman, F. J. Keil, A. Warshel, W. J. Hehre, H. F. S. Iii, J. Kong, A. I. Krylov, P. M. W. Gill and M. Head-Gordon, *Phys. Chem. Chem. Phys.*, 2006, **8**, 3172–3191.

26. G. M. Sheldrick, *Acta Crystallogr. A*, 2008, **64**, 112–122.
27. O. V. Dolomanov, L. J. Bourhis, R. J. Gildea, J. A. K. Howard and H. Puschmann, *J. Appl. Crystallogr.*, 2009, **42**, 339–341.
28. G. M. Sheldrick, *SADABS*, Univ. Gottingen, Germany, 2004.
29. *CrysAlisPro, Version 1.171.36.20 (release 27-06-2012)*, Agilent Technologies.
30. J. Brooks, Y. Babayan, S. Lamansky, P. I. Djurovich, I. Tsyba, R. Bau and M. E. Thompson, *Inorg. Chem.*, 2002, **41**, 3055–3066.
31. J. A. G. Williams, A. Beeby, E. S. Davies, J. A. Weinstein and C. Wilson, *Inorg. Chem.*, 2003, **42**, 8609–8611.
32. M. J. G. Peach, N. Warner and D. J. Tozer, *Mol. Phys.*, 2013, **111**, 1271–1274.
33. T. Ye, J. Chen and D. Ma, *Phys. Chem. Chem. Phys.*, 2010, **12**, 15410–15413.
34. C. Adachi, M. A. Baldo and S. R. Forrest, *J. Appl. Phys.*, 2000, **87**, 8049–8055.
35. S. Lamansky, R. C. Kwong, M. Nugent1, P. I. Djurovich and M. E. Thompson, *Org. Electron.*, 2001, **2**, 53–62.
36. C.-L. Lee, K. B. Lee and J.-J. Kim, *Mater. Sci. Eng. B*, 2001, **85**, 228–231.
37. Q. Liu, L. Thorne, I. Kozin, D. Song, C. Seward, M. D'Iorio, Y. Tao and S. Wang, *J. Chem. Soc. Dalton Trans.*, 2002, 3234–3240.
38. W. Zhuang, Y. Zhang, Q. Hou, L. Wang and Y. Cao, *J. Polym. Sci. Part Polym. Chem.*, 2006, **44**, 4174–4186.
39. C. W. Lee, C. Renaud, P. Le Rendu, T. P. Nguyen, B. Seneclauze, R. Ziessel, H. Kanaan and P. Jolinat, *Solid State Sci.*, 2010, **12**, 1873–1876.
40. C. O. Paul-Roth, S. Drouet, A. Merhi, J. A. G. Williams, L. F. Gildea, C. Pearson and M. C. Petty, *Tetrahedron*, 2013, **69**, 9625–9632.
41. M.-Y. Yuen, S. C. F. Kui, K.-H. Low, C.-C. Kwok, S. S.-Y. Chui, C.-W. Ma, N. Zhu and C.-M. Che, *Chem. – Eur. J.*, 2010, **16**, 14131–14141.

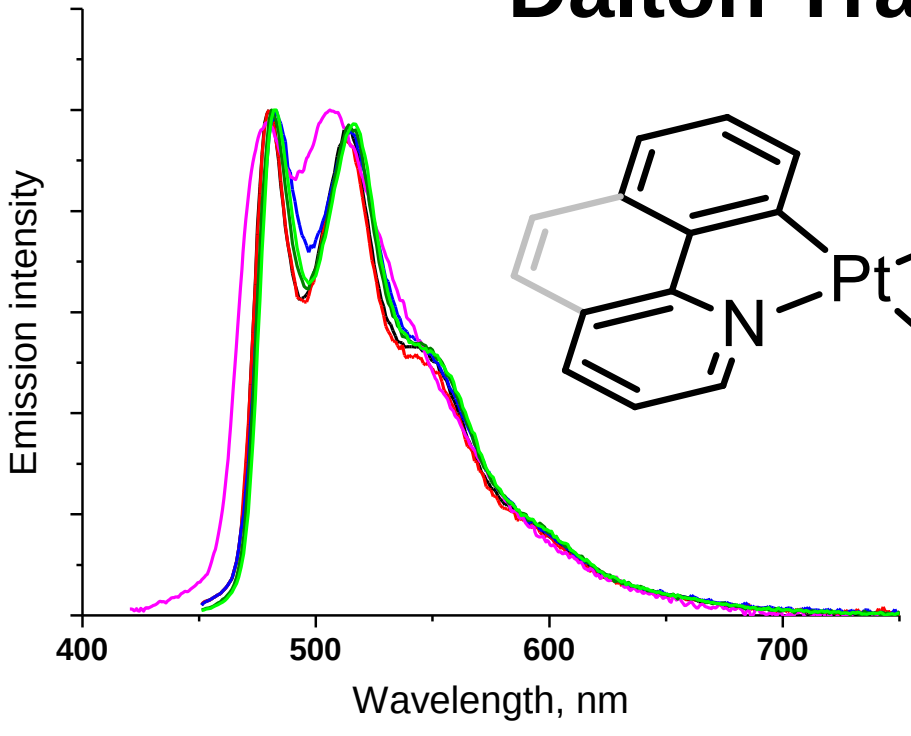

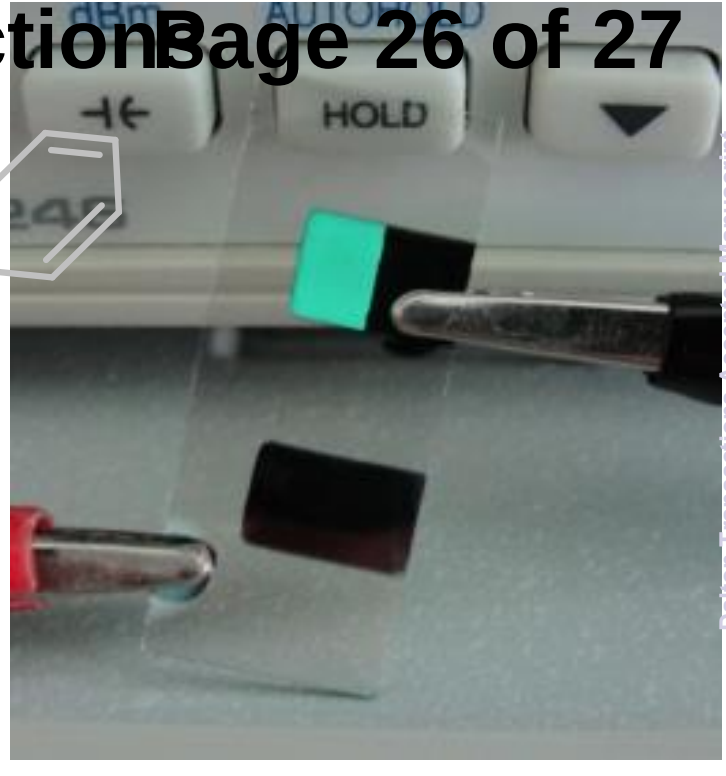

A series of novel NHC Pt (II) orthometallated complexes based on phenylpyridine and benzoquinoline display luminescence ascribed to the IL excited state with a systematic dependence of emission characteristics onto structural parameters of the complexes. The compounds obtained were successfully used to prepare OLEDs with appreciable green emission and good current-voltage characteristics.